JNeurosci
THE JOURNAL OF NEUROSCIENCE

Research Articles: Neurobiology of Disease

Tau isoforms imbalance impairs the axonal transport of the amyloid precursor protein in human neurons

Valentina Lacovich[1,2,#], Sonia L. Espindola[3,#], Matías Alloatti[1,#], Victorio Pozo Devoto[1], Lucas Cromberg[1], Mária #arná[2], Giancarlo Forte[2], Jean-Marc Gallo[4], Luciana Bruno[5], Gorazd B. Stokin[2], M. Elena Avale[3,*] and Tomás L. Falzone[1,6,*]

[1]*Instituto de Biología Celular y Neurociencias (IBCN-CONICET-UBA), Facultad de Medicina, Universidad de Buenos Aires, Argentina.*

[2]*Centre for Translational Medicine (CTM), International Clinical Research Center, St. Anne's University Hospital (ICRC-FNUSA), Brno, Czech Republic.*

[3]*Instituto de Ingeniería Genética y Biología Molecular (INGEBI-CONICET), Buenos Aires, Argentina.*

[4]*Maurice Wohl Clinical Neuroscience Institute, Institute of Psychiatry, Psychology and Neuroscience, King's College London, United Kingdom.*

[5]*Departamento de Física (IFIBA-CONICET), Facultad de Ciencias Exactas y Naturales (UBA), Buenos Aires, Argentina.*

[6]*Instituto de Biología y Medicina Experimental (IBYME-CONICET), Argentina.*

DOI: 10.1523/JNEUROSCI.2305-16.2016

Received: 20 July 2016

Revised: 21 September 2016

Accepted: 4 November 2016

Published: 11 November 2016

Author contributions: V.L., S.E., M.A., V.P.D., L.E.C., M.E.A., and T.L.F. performed research; S.E., M.A., M.C., L.B., M.E.A., and T.L.F. analyzed data; G.F. contributed unpublished reagents/analytic tools; J.M.G., L.B., G.S., M.E.A., and T.L.F. designed research; M.E.A. and T.L.F. wrote the paper.

Conflict of Interest: The authors declare no competing financial interests.

T.L.F and M.E.A acknowledge support from CONICET, University of Buenos Aires and the Argentinean Science Ministry. S.L.E., V.M.P.D., M.A., and L.E.C. receive fellowships from CONICET. This work was supported by grants from MINCyT (PICT 2013-0402, T.L.F and PICT2013-1109, M.E.A.); the Alzheimer Association (NIRG10-172840, T.L.F.), UBA (UBACyT 2011/2014, T.L.F.), the International Brain Research Organization (M.E.A), ISN-CAEN (M.E.A) and European Regional Development Fund - Project FNUSA-ICRC (No. CZ.1.05/1.1.00/02.0123, G.B.S.; LQ1605, G.B.S.). We thank Drs. Mariela Sued and Daniela Rodríguez for help with the statistical analysis of the data; Roux-Ocefa Argentina for kindly contributing with basic reagents and Fundación Rene Baron for donations.

*Corresponding authors: tfalzone@fmed.uba.ar and elena.avale@conicet.gov.ar

Cite as: J. Neurosci 2016; 10.1523/JNEUROSCI.2305-16.2016

Title: **Tau isoforms imbalance impairs the axonal transport of the amyloid precursor protein in human neurons**

One sentence summary: Tau isoforms in APP axonal transport

Authors

Valentina Lacovich[1,2,#], Sonia L. Espindola[3,#], Matías Alloatti[1,#], Victorio Pozo Devoto[1], Lucas Cromberg[1], Mária Čarná[2], Giancarlo Forte[2], Jean-Marc Gallo[4], Luciana Bruno[5], Gorazd B. Stokin[2], M. Elena Avale[3,*] & Tomás L. Falzone[1,6,*].

[1]*Instituto de Biología Celular y Neurociencias (IBCN-CONICET-UBA), Facultad de Medicina, Universidad de Buenos Aires, Argentina.*
[2]*Centre for Translational Medicine (CTM), International Clinical Research Center, St. Anne's University Hospital (ICRC-FNUSA), Brno, Czech Republic.*
[3]*Instituto de Ingeniería Genética y Biología Molecular (INGEBI-CONICET), Buenos Aires, Argentina.*
[4]*Maurice Wohl Clinical Neuroscience Institute, Institute of Psychiatry, Psychology and Neuroscience, King's College London, United Kingdom.*
[5]*Departamento de Física (IFIBA-CONICET), Facultad de Ciencias Exactas y Naturales (UBA), Buenos Aires, Argentina.*
[6]*Instituto de Biología y Medicina Experimental (IBYME-CONICET), Argentina.*

[#]*These authors contributed equally to this work.*

** Corresponding authors: tfalzone@fmed.uba.ar and elena.avale@conicet.gov.ar.*

Number of pages: 39
Number of figures: 5, tables: 1, multimedia: 3 movies
Number of words for Abstract (250), Introduction (650), and Discussion (1494)

Acknowledgements:
T.L.F and M.E.A acknowledge support from CONICET, University of Buenos Aires and the Argentinean Science Ministry. S.L.E., V.M.P.D., M.A., and L.E.C. receive fellowships from CONICET. This work was supported by grants from MINCyT (PICT 2013-0402, T.L.F and PICT2013-1109, M.E.A.); the Alzheimer Association (NIRG10-172840, T.L.F.), UBA (UBACyT 2011/2014, T.L.F.), the International Brain Research Organization (M.E.A), ISN-CAEN (M.E.A) and European Regional Development Fund - Project FNUSA-ICRC (No. CZ.1.05/1.1.00/02.0123, G.B.S.; LQ1605, G.B.S.). We thank Drs. Mariela Sued and Daniela Rodríguez for help with the statistical analysis of the data; Roux-Ocefa Argentina for kindly contributing with basic reagents and Fundación Rene Baron for donations. The authors declare no competing financial interests.

Abstract.

Tau, as a microtubule-associated protein, participates in key neuronal functions such as the regulation of microtubule dynamics, axonal transport and neurite outgrowth. Alternative splicing of exon 10 in the tau primary transcript gives rise to protein isoforms with three (3R) or four (4R) microtubule binding repeats. While tau isoforms are balanced in the normal adult human brain, imbalances in 3R:4R ratio have been tightly associated to the pathogenesis of several neurodegenerative disorders, yet the underlying molecular mechanisms remain elusive. Several studies exploiting tau overexpression and/or mutations suggested that perturbations in tau metabolism impair axonal transport. Nevertheless, no physiological model has yet demonstrated the consequences of altering the endogenous relative content of tau isoforms over axonal transport regulation. Here we addressed this question using a *trans*-splicing strategy that allows modulating tau exon 10 inclusion/exclusion in differentiated human-derived neurons. Upon changes in 3R:4R tau relative content neurons showed no morphological changes, but live imaging studies revealed that the dynamics of the amyloid precursor protein (APP) were significantly impaired. Single trajectories analyses of the moving vesicles showed that predominance of 3R tau favored the anterograde movement of APP-vesicles, increasing anterograde run lengths and reducing retrograde runs and segmental velocities. Contrarely, the imbalance towards the 4R isoform promoted a retrograde *bias* by a significant reduction of anterograde velocities. These findings suggest that changes in 3R:4R tau ratio has an impact on the regulation of axonal transport and specifically in APP dynamics, which might link tau isoforms imbalances with APP abnormal metabolism in neurodegenerative processes.

Significance statement: Tau protein has a relevant role in the transport of cargos throughout neurons. Dysfunction in tau metabolism underlies several neurological disorders leading to dementia. In the adult human brain, two tau isoforms are found in equal amounts, while changes in such equilibrium have been associated with neurodegenerative diseases. We investigated the role of tau in human neurons in culture and found that perturbations in the endogenous balance of tau isoforms were sufficient to impair the transport of the Alzheimer's disease related APP, although neuronal morphology was normal. Our results provide evidence of a direct relationship between tau isoforms imbalance and defects in axonal transport, which induce an abnormal APP metabolism with important implications in neurodegeneration.

Introduction.

The microtubule-associated protein tau regulates microtubules (MTs) dynamics supporting the axonal transport of proteins, vesicles and organelles (reviewed in Morris et al. 2011). A number of neurodegenerative diseases referred to as tauopathies, including Alzheimer's Disease and some forms of Frontotemporal Dementia, are characterized by the aberrant accumulation of hyperphosphorylated tau. In such pathological conditions tau is disengaged from MTs and accumulated in insoluble filamentous inclusions (reviewed in Spillantini & Goedert 2013).

The human *MAPT* gene encoding tau protein comprises 16 exons. Alternative splicing of exons 2, 3 and 10 produces six different isoforms in the central nervous system (Goedert et al., 1989). Exon 10 (E10) encodes the second of four microtubule-binding repeats; thus, E10 alternative splicing gives rise to tau isoforms with three (3R) or four (4R) MT-binding repeats (Goedert et al., 1989). Only 3R tau is expressed in the

85 developing brain while a balanced 3R:4R tau expression is found in the adult human
86 brain (Goedert et al., 1989; Andreadis, 2005). Mutations impairing E10 splicing
87 segregate with disease in familial frontotemporal dementia with parkinsonism linked to
88 chromosome 17 (FTDP-17) (Hutton et al., 1998; Spillantini et al., 1998). To date, more
89 than 50 disease-associated mutations have been found in *MAPT*, with a third of them
90 affecting E10 splicing (Ghetti et al., 2015). Yet, the mechanisms underlying
91 neurodegeneration due to 3R:4R isoform imbalance remain to be further elucidated.

92 Among the myriad of neuronal functions affected by tau abnormal metabolism,
93 axonal transport is likely to be particularly disturbed: The anterograde and retrograde
94 axonal transport of cargos is mediated by kinesin and dynein motors that differentially
95 interact within the MT-polarity (Terada et al., 2010; Encalada and Goldstein, 2014). Tau
96 can regulate axonal transport either by directly interacting with molecular motors, by
97 altering MT dynamics or competing with the binding of motors to MT (Dixit et al., 2008 ;
98 Kanaan et al., 2012; Goldstein, 2012). Tau-microtubule interaction depends on the
99 number of tau microtubule-binding domains (Panda et al., 2003) thus, it is potentially
100 affected by the relative content of 3R and 4R isoforms, as well as by mutations in E10.
101 Transgenic mice expressing missense human E10 mutations (P301S or P301L)
102 revealed deficits in axonal transport (Ittner et al., 2008; Bull et al., 2012; Mellone et al.,
103 2013; Rodríguez-Martín et al., 2016). Conversely, reduction in the level of kinesin-I
104 anterograde motor enhance tau pathology in the P301L transgenic mouse, suggesting
105 that transport defects impact on tau physiology (Falzone et al., 2009). Also, cultured
106 neurons showed mitochondrial axonal transport defects under 3R or 4R isoform

overexpression (Stoothoff et al., 2009; Mertens et al., 2013) or when bearing mutations that increase E10 inclusion (Iovino et al., 2014).

The amyloid precursor protein (APP) is significantly linked to Alzheimer's Disease, leading to the generation of amyloid-β and plaque pathology under the presence of mutations, overexpression or transport defects (Stokin et al., 2005; Goldstein et al. 2012). As a Golgi-derived transmembrane protein, APP-vesicles undergo constitutive fast axonal transport, interacting with kinesin and dynein motors (Reis et al, 2012, Fu and Holzbaur, 2013, Koo et al, 1990). Defects in APP transport are early events in neurodegenerative diseases (Stokin et al., 2005; DeVos et al, 2008), therefore, measuring APP dynamics is a gold standard method for detecting transport deficits associated with pathological conditions (Goldsbury et al., 2007; Falzone and Stokin, 2012).

In this study we investigated whether the imbalance in 3R:4R ratio impact on the dynamics of APP axonal transport in human neurons. We used a *trans*-splicing RNA reprogramming strategy that drives the inclusion/exclusion of exon 10 in the endogenous tau transcript (Avale et al., 2013). Tau isoforms ratio was modulated without altering total tau protein amount in cultured differentiated neurons derived from human embryonic stem cells (hESC). Live imaging analyses of APP fluorescent vesicles revealed differential effects of 3R or 4R isoforms over anterograde and retrograde axonal transport, suggesting that changes in endogenous tau isoform ratio impairs APP transport in human neurons.

Materials & Methods

Cell culture and neuronal differentiation

Neurons were derived from hESCs. Briefly, irradiated MEFs were plated over gelatin coated Petri dishes 24h prior to hESCs plating and maintained in DMEM complete (high glucose DMEM, 10% FBS, 1% Glutamax, 1% penicillin-streptomycin). hESCs were grown at 37°C, 95% humidity and 5% CO_2 in Human Embryonic Stem Cell media (KO DMEM, 20% KO Serum Replacement, 1% Glutamax, 1% Non Essential Amino Acids, 0.1% Beta-Mercaptoethanol, 4 ng/ml bFGF) to allow colony formation. When colonies reached optimal size they were first transferred to a Petri dish and after 12-18 hours to 25 cm^2 flasks and grown in suspension to allow embryoid body formation, which was induced by Neural Induction Media NIM (DMEM/F12, 1% N2 Supplement, 1% of Non-essential AA, 280UI/ml heparin and 1% penicillin-streptomycin). Embryoid bodies were then transferred to laminin coated 6 multi-well plates for neural rosettes formation. After 7-14 days of growth, the neural rosettes were picked and transferred to 25 cm^2 flasks and maintained in NIM complete medium (NIM, 2% B27 supplement, Ascorbic Acid) for up to one month, changing the growth medium every two days. Neural rosettes were picked and dissociated by a 5 min Accutase and Trypsin treatment. The reaction was blocked by Trypsin inhibitor and the suspension centrifuged for 5 min at 1000 rpm. The pellet was washed with DMEM/F12 and resuspended in Neural Differentiation Media NDM (Neurobasal, 1% N2 supplement, 2% B27 supplement and 1% penicillin-streptomycin). Cells were plated over poly-ornitine and laminin coated coverslips into 24-multiwell plates and maintained in 500 µl/well NDM complete medium (NDM, Laminin, cAMP, Ascorbic Acid, BDNF, GDNF).

154

155 *Neuron plating, transduction and transfection*

156 Plated neurons were maintained in culture, changing ¾ of the medium every 7 days. On
157 DIV11 neurons were transduced with either control (dsRED), PTM-4R (formerly named
158 PTM6)(Rodriguez-Martin et al., 2005) or PTM-3R (formerly PTM9)(Rodriguez-Martin et
159 al., 2009). PTMs were expressed under the human synapsin promoter, in a replication-
160 defective lentiviral vector, prepared as described previously (Avale et al., 2013). 5 µl of
161 each concentrated LV (~10^7 TU/ml) were added in 200 µl medium per well containing
162 150,000 neurons, to achieve a multiplicity of infection (MOI) between 5 to 10, as
163 previously described (Avale et al., 2013)). After 12 hours the cells were topped up with
164 300 µl of fresh NDMc medium. Seven days after LV transduction (on DIV18), neurons
165 were transfected with 1 µg of pcDNA3-APP-YFP (Falzone et al., 2009) in a transfection
166 mix of OptiMEM and Lipofectamine 2000.Two hours after transfection, culture medium
167 was replaced and 24 hours later (on DIV 19) neurons were analyzed by imaging for
168 transport analysis, fixed for immunocytochemistry or processed to obtain RNA and
169 protein for qPCR and western blot analyses. *3R and 4R Tau Isoform quantitation by*
170 *qPCR*

171 Total RNA was isolated from neurons using AllPrep DNA/RNA mini kit (Qiagen) from
172 high density cultures at DIV 19. Reverse transcription was performed with 0.5 µg of
173 RNA with the TaqMan RT kit (Applied Biosystems) in a total volume of 10 µl. RT
174 conditions were: 10 min at 25°C, 30 min at 48°C, and 5 min at 95°C. To simultaneously
175 detect tau isoforms by end-point PCR, 0.2 µg of reverse-transcribed RNA were
176 amplified by PCR using Go Taq polymerase (Promega) with primers spanning exons 9-

13, as previously described (Avale et al., 2013). PCR products were separated by electrophoresis in 2% (w/v) agarose gels and stained with ethidium bromide. To perform the relative quantification of 4R and 3R mRNA isoforms by real time PCR, specific pairs of primers were used for each isoform, annealing with the E9-E10 or the E9/11-E11 junction. Both pairs of primers showed similar efficiency. Primer sequences were as follows: *4Rfor*(E9):*5'*TCCACTGAGAACCTGAAG*3'*; *4Rrev(E10):*5'AGTGTGGCTCAAAGGATA*3'*; *3Rfor(E9/11):5'*AGGCGGGAAGGTGCAAATAG*3'*;*3Rrev(E11)*:*5'*TCCTGGTTTATGATG GATGTT*3'.* The mRNA coding for human Apolipoprotein B was used as a reference (*ApoBFor:5'*-TGGTGCTCACAAGGCGACACTAA3´; *ApoBRev*:*5'*GGCGGCTTTCCCATCCAGACTA-3´). Real-time PCR reactions were performed in triplicate with 10 ng of cDNA and 5 µl of Power SYBR® Green PCR Master Mix (Applied Biosystem) in a final volume of 10 µl using a MJ Research Opticon 2 thermal cycler under the following cycling conditions: initial denaturation at 95°C for 3 min, 50 cycles of 30 s at 95°C, 30 s at 58°C and 45 s at 72°C, and a final step of 1 min at 72°C. Data was analyzed with the *Opticon monitor 3* software (Biorad) to obtain the ΔCt per sample (Ct Tau isoforms-Ct ApoB). Data from three independent experiments were pooled and analyzed using Graph Pad Prism software.

Western blotting

Total protein was collected from neurons at DIV19 in 100 ul of sample buffer (40 mM Tris-HCl (pH 7,5), 150 mM NaCl in 1× protease inhibitor (Invitrogen). Protein concentration was measured using the Bradford assay (Bio-Rad). Equal amounts of protein (10-20 µg) in 20 µl of loading buffer (bromophemol blue (0.5 %), 10 % glycerol

and 10% of 2-Mercaptoethanol) were loaded onto 12% (w/v) SDS-polyacrylamide gels (N,N`-Methylenebisacrilamide 30%, Invitrogen). Proteins were transferred onto nitrocellulose membranes (Whatman, USA) using the wet transfer method. Membranes were blocked in 5% (w/v) nonfat milk (Sancor, Argentina), 0.05% v/v Tween 20 in PBS for 1 hour. After blocking, membranes were incubated overnight at 4°C in blocking solution containing primary antibody directed against 3R Tau (1:2000 Anti-Tau 3-repeat isoform RD3; mouse monoclonal, Millipore), 4R tau (1:1000 Anti-Tau 4-repeat isoform RD4; mouse monoclonal, Millipore), total tau (1:10000; rabbit polyclonal; SIGMA), phosphorylated tau CP13 and PHF1 (1:200; gift from Dr. Peter Davies), β-actin (mouse monoclonal, 1:10000; abcam), APP (mouse monoclonal 22C11) or tubulin (mouse monoclonal, 1:800, DM1a, Covance). After washing 3 times in TBS containing 0.05% v/v Tween 20, blots were incubated with the appropriate secondary antibody, goat anti-rabbit (1:2000, Cell Signaling) or horse anti-mouse (1:2000, Cell Signaling) for 3 hours at room temperature. Proteins were visualized using the GeneGnomeXRQ (Syngene, US). Scanned images were analyzed using ImageJ software.

Imaging, tracking and analysis

Imaging of live cells and kymograph analysis of axonal transport was carried as previously described (Falzone and Stokin, 2012). Briefly, 30s movies of APP–YFP moving particles in neurons were recorded by using an inverted epifluorescence microscope (Olympus IX81) connected to a CCD camera (Olympus DP71/12.5 megapixels). Cultures were observed under a 60x lens (NA: 1.40) and maintained at 37˚C, 5% CO_2 and 10% humidity using a CO_2 humid chamber and heated stage

(Olympus). Directionality was determined by tracking fluorescent axons. To avoid introducing biases due to the gradient concentration of tau in axons, imaging was performed in axons at their middle part separated by at least 2 fields of view distance (~200 µm) from cell bodies and from axonal tips. Kymographs were generated from the recordings with ImageJ using the multiple kymograph plug-in (Otero et al., 2014) and processed using Image-Pro Plus 6 (Media Cybernetics, Rockville, MD, USA) and MATLAB scripts (The Mathworks, Natick, MA, USA) to track single fluorescent vesicles with sub-pixel precision, as previously reported (Otero et al., 2014). Kymographs were blind-coded for particle tracking and unbiased data collection.

Segmental velocities, run-lengths, pauses and reversions were computed from trajectories using custom made MATLAB routines. For the calculation of segmental velocities, processive trajectories were divided into segments and the mean velocity of the segment was computed from the slope using a MATLAB algorithm. Briefly, each trajectory was cut in segments of 20 frames of duration producing a linear approximation with the least squares method, filtering trajectories with outliers and significant differences between the dataset and the fitted curve. Subsequently, the slope of the regression was considered as the velocity of the segment. The point in which the movement is equal to 0, filtering the points produced by the noise of the trajectory was used for the calculation of run-lengths, pauses and reversions. The trajectories between those points are considered continuous segments and classified in anterograde or retrograde movement if they show positive or negative velocity respectively (velocities are the slope of a linear approximation of the trajectory). Pauses are considered when segments follow a stationary criteria for more than 5 frames (625 ms) moving less than

246 0.05 pixel per frame (<0.16 μm/sec). The script merges continuous segments of the
247 same type, and segments that are too small. The difference in μm between the final
248 point and the initial point of a determined continuous segment is considered as the run-
249 length. The points separating anterograde and retrograde segments are considered
250 reversions. The parameters of the Gaussian mixture model were determined by an
251 Expectation Maximization (EM) algorithm using a function (gmdistribution.fit) in
252 MATLAB. A bootstrapping with resampling procedure with N=1000 was implemented to
253 compute the intervals of confidence of the Gaussian mixture parameters estimates.
254
255 *Immunofluorescence, image collection and morphology*.
256 Cells were washed with phosphate-buffered saline (PBS), and fixed with 4% para-
257 formaldehyde and 4% sucrose in PBS for 30 minutes at 37°C. After fixation cells were
258 washed twice with PBS for 10 minutes and permeabilized with 0.1% Triton X-100 for 10
259 min at room temperature. Cells were incubated at room temperature for 1 h using a
260 blocking solution consisting of 3% bovine serum albumin (BSA), 0.1% Triton X-100 and
261 10% goat serum in PBS. Cells were then stained with primary antibodies in blocking
262 solution and incubated overnight at 4°C. When using two primary antibodies, the
263 staining was done sequentially. Cells were then rinsed in PBS and stained with
264 secondary antibodies at room temperature for 2 hours. Cells were stained for 30 min
265 with Hoechst and mounted on slides with 70% glycerol. Primary antibodies used were:
266 anti tau CP13 (1:800), rabbit polyclonal to total tau (1:800), APP (1:800) and secondary
267 antibodies against mouse and rabbit IgG conjugated to Alexa Fluor 564 (1:400) or Alexa
268 Fluor 488 (1:400). Fixed cells were imaged with an inverted Zeiss LSM 780 confocal

269 microscope (Zeiss, Oberkochen, Germany) using an oil immersion objective (40×/0.55
270 N.A). YFP fluorescence was excited by 488 nm line of the argon laser, while the
271 emission light was collected through the band pass filter (505-530 nm). Red
272 fluorescence (dsRED) was excited with the He/Ne laser (543 nm) and the emission light
273 was filtered with long pass filter, with a cut-off below 560 nm. Neuronal morphology was
274 quantitatively evaluated with three parameters which describe neuron size and
275 projection branching complexity. Briefly, the projection extension was estimated by
276 measuring the sum of all the projections from images of single neurons imported in
277 Image J after pixel was converted into μm. The skeletonized neuron length was
278 estimated from total extensions and number of primary projections obtained. Branching
279 complexity was investigated using the Sholl plug-in in Neuron-J from which number of
280 intersections along consecutive rings was obtained and represented in plots of
281 projection intersection versus soma distance in μm. Statistical significance of data was
282 determined with the two-tailed *t* test. Values are expressed as Mean ± S.E.M.
283

Results:

Modulation of 3R:4R tau ratio by *trans*-splicing in differentiated human neurons

Neuronal cultures were obtained by differentiation of human embryonic stem cells (Hues9) using a standard protocol previously described (Figure 1; Zhang et al. 2010). To test for proper polarization, immunofluorescence staining was performed 5 days after plating (DIV 5); at this stage human neurons showed early development of highly polarized structures with defined axonal (tau-positive) and dendritic (MAP2-positive) projections (Figure 1B). After 19 days in culture (DIV 19), enriched neuronal cultures displayed dense connectivity and axonal arborization together with detectable staining of tau in the axons (Figure 1C). At this stage, neurons also show electrophysiological profiles of mature neurons such as repetitive spiking and increased amplitude of voltage-dependent Na^+ and K^+ currents (Pozo Devoto, *et al*.; under revision).

To modulate the relative content of 3R:4R tau isoforms, we used a *trans*-splicing RNA reprogramming strategy (Rodriguez-Martin et al., 2005). Tau pre-*trans*-splicing molecules (PTMs) were delivered using lentiviral vectors (LV), as previously described (Avale et al., 2013). After integration into the neuron genome, the PTM cassette is transcribed into an RNA molecule that binds to intron 9 of the endogenous tau transcript and drives a *trans*-splicing reaction (Figure 1E). We used two different LVs carrying Tau-PTMs: i) LV-Tau-PTM3R, containing exons 11-13 to exclude exon 10 from the tau transcript; or ii) LV-Tau-PTM4R, carrying exons 10-13 to include exon 10 in the resulting *trans*-spliced product (Figure 1E). Based on this strategy, LV-PTM3R is expected to increase the relative content of 3R tau, while LV-PTM4R would drive the production of 4R tau (Figure 1E). High density neuronal cultures were transduced at DIV 11 with LV-

Tau-PTM3R, LV-Tau-PTM4R or LV control, carrying a red fluorescent reporter gene (dsRED) instead of the PTM, within the same vector backbone (Figure 1E). Molecular, immunofluorescence and functional analyses were performed at DIV 19, to allow maximal expression of the LVs. Transduction efficiency was assessed by the expression of the fluorescent reporter dsRED from the control LV (Figure1D).

To validate the *trans*-splicing system in human derived neurons we first analyzed 3R and 4R tau isoforms measuring the relative content of tau mRNA with or without E10 (here after also referred to as 4R and 3R mRNA, respectively) (Figure 1F-G). End point RT-PCRs, using primers that amplify both isoforms simultaneously from RNA of transduced neurons, showed a clear change in tau isoforms relative content in either PTM transductions compared with control (Figure 1F). We next performed a relative quantification analysis by real time RT-PCR, using isoform-specific primers to analyze changes in 3R and 4R relative contents (Figure 1G, see methods). Control neurons at DIV 19 showed a 4R/3R ratio of 0.6 ± 0.07, suggesting neuronal maturity evidenced by the presence of 4R tau, although the 3R:4R isoform balance was not yet achieved at this stage. As expected, transduction with LVs carrying either PTM3R or PTM4R induced a bias in the endogenous 4R/3R ratio: LV-PTM3R transduced neurons showed a net 4R/3R tau ratio reduction to 0.34± 0.17 due to a 30% relative increase in 3R tau, although the reduction observed in 4R isoform was not statistically significant. On the other hand, LV-PTM4R transduced neurons showed 2-fold increase in 4R tau compared to control neurons, while a 50% reduction in 3R tau was observed, yielding a relative 4R/3R ratio increase to 3.9 ± 0.18 (Figure 1G).

To test whether the change in the relative content of tau isoforms observed at the RNA level was translated to the protein content, 3R and 4R tau were separately detected by western blotting with isoform-specific antibodies in protein lysates obtained at DIV19 from each LV transduced neurons (Figure 1H-I). Due to potential differences in antibodies affinities it is not possible to accurately estimate the 4R/3R tau ratio at the protein level, then, changes in each tau isoform were analyzed independently, comparing PTM transduced neurons *versus* control conditions. Neurons transduced with LV PTM3R showed a significant increase in 3R tau protein amount compared to transduction with the control virus (Figure 1H) with a mild reduction observed in this isoform under PTM4R transduction. Conversely, 4R tau protein content (Figure 1I) was increased after PTM4R transduction and decreased in PTM3R transduced neurons. Taken together, these results suggest that the *trans*-splicing strategy was efficient to modulate the relative content of tau isoforms in differentiated neurons, both at the RNA and protein levels.

Normal neuronal polarization in human derived neurons under 3R:4R tau isoform imbalance.

We next evaluated whether changes in tau isoform ratio impacts on neuronal survival and/or morphology. Neuronal structure and polarization in transduced neurons were analyzed by immunofluorescence staining against cytoskeletal and membrane markers at DIV 19 (Figure 2 A,B). Tau and APP staining showed similar number of neurons in LV-PTM3R and LV-PTM4R transduced cultures compared with non-transduced control (NTC), displaying similar degree of ramification and arborization (Figure 2 A, B). In

addition, no changes in the number of projections or differences in axonal or dendrite length were observed between control and LV-PTM3R or LV-PTM4R transduced neurons (Figure 2C-E). Transduced neurons did not show evidence of axonal retraction or swelling, neither the accumulation of tau in their projections (Figure 2B). These results indicate that neither the transduction with LVs nor the induced changes in tau isoforms ratio alter survival, polarization or morphology of human neurons in culture.

To test whether PTM expression, or the LV transduction, alter the amount of total tau protein we performed western blot analysis from homogenates collected at DIV 19 using an anti-tau or anti-APP antibody. No changes in the amount of total tau or APP were observed between control (dsRED), LV-PTM3R and LV-PTM4R transduced neurons (Figure 2 F, G), showing that neither LV transduction nor the modulation of tau isoforms alter the total content of these proteins. To test whether a shift in tau isoforms balance might induce changes in tau phosphorylation we also performed western blot analyses using antibodies recognizing tau phosphorylated at Ser202 (CP13) or at Ser 396/404 (PHF1). No differences were observed among the experimental conditions suggesting that the level of tau phosphorylation is not affected after *trans*-splicing (Figure 2H). Therefore, through the use of the *trans*-splicing strategy we have been able to modulate the relative 3R:4R tau ratio in differentiated human neurons without altering tau protein expression, phosphorylation state, neuronal morphology, or survival. We thus reasoned that this is a suitable model to investigate particular neuronal functions, such as axonal transport, that might be affected by tau isoforms imbalance.

APP axonal transport impairment after changes in the 3R:4R tau ratio.

Since the 3R:4R tau ratio can be efficiently modulated by *trans*-splicing, we next asked whether imbalance in tau isoforms perturbs APP axonal transport. To answer this question APP dynamics was monitored at DIV19 by continuous high definition live imaging recordings to generate movies from axons identified by morphology, as previously described (Otero et al., 2014). Neurons were transduced at DIV11 with LV-PTM3R, LV-PTM4R or control LV-dsRED and transfected at DIV18 with the fluorescent hAPP695-YFP expression vector (pCDNA3-APP-YFP) to track fluorescent APP vesicles as indicated in the experimental timeline (Figure 1). Co-localization of YFP and dsRED signals in transduced control showed that 99% of APP-YFP transfected cells were also transduced with the LV (Figure 1D). A group of neurons that had not been transduced with LVs (non-transduced control, NTC) was also included in the experiment to rule out any effect over APP transport due to LV transduction. Movies were obtained from axons at their middle part (at least 200 µm away from the cell body or tip) to generate detailed kymographs of time *versus* distance, for qualitative and quantitative analyses (Figure 3A, see movies 1-3). The parameters analyzed (velocities and run lengths) of APP dynamics in control (NTC) neurons were comparable to those described for different neuronal settings from mouse, chicken and *Drosophila* with vesicular movement undergoing fast anterograde and retrograde axonal transport (Goldsbury et al., 2007; Reis et al, 2012; Falzone and Stokin, 2012). NTC human neurons revealed an even distribution of anterograde and retrograde moving APP vesicles and a fraction of stationary vesicles under the time frame analyzed (Figure 3C). The average velocity for anterograde and retrograde APP moving vesicles in NTC conditions (Figure 3D) were

consistent with the values obtained for fast axonal transport in other systems (Stokin et al., 2005; Falzone et al., 2009).

Transduction with either LV-PTM3R or LV-PTM4R significantly impaired the axonal transport of APP (Figure 3C). More specifically, increased levels of 3R isoform (by LV-PTM3R transduction) led to 30 - 50 % reductions of anterograde and retrograde APP movement respectively; and significantly increased the proportion of stationary vesicles by 30% (Figure 3C). Interestingly, shifting the balance towards 4R isoform (LV-PTM4R transduction) produced a similar reduction of the APP anterograde and retrograde transport while increasing the stationary proportion (Figure 3C). The density of APP-YFP vesicles in axons was similar between the different conditions (Figure 3E), revealing that the observed reduction in transport is likely to be induced by a shift from moving towards stationary vesicles. When analyzing the dynamics of net moving vesicles of APP-YFP, anterograde and retrograde average velocities (including movement and pauses of each analyzed particle) were significantly reduced in LV-PTM3R and LV-PTM4R transduced neurons compared with dsRED or NTC neurons (Figure 3D). Control transduced (LV-dsRED) neurons showed similar proportions and average velocities of APP-YFP vesicles compared with control NTC neurons, suggesting that LV transduction itself does not modify APP axonal transport properties measured 8 days post transduction (Figure 3C, D). Taken together, these results showed significant changes in the movement of APP vesicles when the endogenous ratio of 3R:4R tau isoforms is modified, suggesting that axonal transport of APP is tightly regulated by the ratio of tau isoforms, either attached to MTs or soluble in the axonal shaft.

Differential anterograde and retrograde regulation over APP axonal transport by 3R or 4R Tau isoforms

To further understand tau regulation over APP transport dynamics in human neurons and to investigate potential mechanisms affected by the 3R:4R imbalance, fluorescent APP moving vesicles were tracked using an algorithm developed to identify particle positions with sub-pixel precision. Single trajectories obtained from movies (Figure 3 A, B) were analyzed using custom made MATLAB routines in order to extract axonal transport properties such as run length, number of pauses per trajectories, reversion of directionality and segmental velocity distributions (see methods, Figure 4). To understand whether tau can regulate processive axonal transport of APP we computed the anterograde average run length of APP vesicles in LV-PTM3R and LV-PTM4R transduced neurons and compared them with control transduced neurons (Figure 4C). Interestingly, shifting tau isoforms towards 3R content (LV-PTM3R) induced a significant (30%) increase of the anterograde run length but enhancing 4R isoform (LV-PTM4R) showed no significant effect on anterograde runs (Figure 4C). On the other hand, LV-PTM3R transduction induced a significant effect on the retrograde component with more than 70% reduction in the average run length while LV-PTM4R showed no changes over the average retrograde run length compared with control conditions (Figure 4C). We did not observe significant changes in the number of pauses within trajectories and in reversion from anterograde to retrograde transport or *vice versa* due to tau 3R:4R shifting (Figure 4D). Next, we analyzed the distribution of segmental velocities of moving APP vesicles in LV-PTM3R, LV-PTM4R compared with control transduced

neurons (Figure 4E, F). A multimodal distribution of segmental velocities was observed, thus we propose a Gaussian mixture model with 3 components to describe each data set (see methods, and Reis et al. 2012). The distribution of anterograde segmental velocities in control transduced neurons ranges from 0.1 to 5 μm/second and can be adjusted to modes A, B and C (Figure 4E). A similar result was obtained for the distribution of retrograde segmental velocities, but with more probable lower velocities (Figure 4F). The distributions obtained from neurons transduced with either LV-PTM3R or LV-PTM4R showed that anterograde segmental velocities are affected by shifting tau ratios either towards 3R or 4R (Figure 4E, F and Table I). Enhanced 3R content showed mild shape changes in the anterograde segmental velocity distribution revealing reduced modes of velocities mainly in the C mode with enhanced representation for mode A (Figure 4E, Table I). On the other hand, shifting tau content towards 4R induced significant reductions in anterograde velocities for modes A, B and C compared with control and with LV-PTM3R transduction (Figure 4E). Under 3R increase, the amplitude of anterograde modes A and B were significantly increased suggesting also a shift in the total distribution to lower anterograde velocities (Figure 4E, table I). Retrograde axonal transport of APP under enhanced 3R isoform showed significant changes of retrograde segmental velocity distributions compared with control (Figure 4F). Nevertheless, no change in the number of segmental velocities representing each mode pick (mode weight) was observed in LV-PTM3R transduced neurons (Figure 4F, Table I), suggesting that increases in 3R tau induce mild reductions in the dynein movement, affecting the retrograde component. Neurons transduced with LV-PTM4R showed less impact on the retrograde movement with similar retrograde modes

compared with control, however, enhanced mode weights were observed for mode A, with significant weight reductions for modes B and C (Figure 4F, table I). Taken together, these results suggest that changes in tau isoform ratio towards increases either in 3R or 4R can directly modulate the properties of anterograde and retrograde APP vesicles movement by differentially changing the run length and modifying the distribution of segmental velocities of moving vesicles.

Discussion

Here we tested whether relative content in tau isoforms played crucial roles in the regulation of axonal transport, combining the RNA *trans*-splicing strategy with high definition/speed live imaging of APP vesicles in human-derived neurons. Our findings have particular relevance to understand early neuronal dysfunction and the interplay between tau and APP in molecular pathways of disease (Götz et al., 2006; Goldstein 2012).

Axonal transport is one of the tau-regulated mechanisms likely perturbed in tauopathies, yet the available data seems controversial. On one hand, several experimental models showed axonal cargo depletion, clogging and transport defects after tau overexpression (Ebneth et al., 1998; Stamer et al., 2002; Mertens et al., 2013). Moreover, impairments in transport dynamics have been observed under abnormal tau 3R:4R content in cultured neurons (Iovino et al., 2015; Mertens et al., 2013, Stoothoff et al., 2009) and in mouse models (Dawson et al, 2007). However, tau overexpression or disease-associated mutants might have underlined some of the observed phenotypes, making difficult to determine the precise role of tau isoform ratio in transport. On the

other hand, some experiments showed no defects in ^{35}S-methionine-labeled protein distribution in tau knock-out mouse models, suggesting that tau deletion or overexpression might not influence transport (Yuan et al., 2008; Yuan et al., 2013). However, it has been shown that tau knock-out mice upregulate other MAPs as a compensatory mechanism, (Ke et al., 2012; Ma et al., 2014), which may account for the lack of transport deficits in those mice. Furthermore, it is particularly difficult to analyze the role of 3R:4R tau balance in mice because only 4R tau is expressed in the adult rodent brain. The *trans*-splicing strategy have created a unique platform to dissect the functional consequences of human tau isoform imbalance, allowing the modulation of the endogenous tau isoform ratio in differentiated human neurons, without altering total tau protein or impairing other tau-dependent functions such as axon elongation or neuronal polarization.

Axonal transport defects underlie many neurological diseases (Stokin et al., 2005 DeVos et al., 2008; Goldstein 2012). However, it remains unclear whether such impairments represent an early causative effect or a late consequence in disease (Götz et al., 2006; Goldstein, 2012; Bodea et al., 2016). Particularly, the transport of APP and its subcellular *mis*-localization have putative implication in Alzheimer's Disease, with tau playing a crucial role in controlling APP trafficking (Stamer et al., 2002; Goldsbury et al., 2007). Here we show that changes in the endogenous 3R:4R tau ratio are sufficient to significantly impair the transport of APP vesicles in human neurons suggesting a possible pathological link between tau isoform imbalances and APP. These results open new avenues to understand how tau isoforms modulate not only the dynamics but also

511 the metabolism of APP, that is intimately linked to its intracellular transport (Rodrigues
512 et al., 2012).

513 From a mechanistic perspective, our data complement previous evidence about
514 the role of tau in the regulation of molecular motors. Two models have been proposed
515 for the bidirectional transport of cargos such as APP vesicles along MTs: *Coordination,*
516 assumes that anterograde kinesin and retrograde dynein motors activity are regulated
517 by accessory proteins, and thus the direction of motion depends on which motor is
518 active (Fu and Holzbaur, 2013; Leidel et al., 2012); and *tug-of-war,* which postulates
519 that cargo direction is exerted by the larger net force resulting from both polarity motors
520 simultaneously active (Müller et al., 2008). Recently, a hybrid interaction between both
521 models is proposed to lead transport (Hendricks et al., 2012). The many physiological
522 roles of tau can modulate transport by regulating motor-microtubule interaction
523 (Trinczek et al., 1999; Magnani et al., 2007), modifying the MT structure and/or
524 triggering phosphorylation cascades that modify motors (Kanaan et al., 2012). In this
525 context, we propose that APP vesicles are bound to multiple kinesin and dynein motors
526 which are regulated by tau (Figure 5). Tau binding transiently to MTs increases the
527 probability of kinesin detachment (Dixit et al., 2008), and if tau concentration is high, the
528 probability of unbound kinesin to attach to the MT is reduced (Vershinin et al., 2007)
529 (Trinczek et al., 1999). Conversely, dyneins are less affected by tau on MT (Dixit et al.,
530 2008). Thus, we propose that under balanced content of 3R:4R tau, few weak dyneins
531 and stronger kinesins would transport the APP vesicle, resulting in control values of run
532 lengths and segmental velocities (Figure 5A). Based on binding results showing that the
533 affinity of 3R isoform for MTs is lower than that of 4R (Goode et al., 2000) and assuming

that affinity is directly related with the mean attachment time of tau on a MT, we propose that the 3R increase enhances the number of active motors driving the cargo, although the number of sites occupied by tau within the MT would remain equal. Then, the engagement of extra kinesins would lead to enhanced anterograde processivity (longer runs). The reduction in retrograde runs and segmental velocities in 3R are also consistent with this model, since kinesin could act as a dynein anchor (Figure 5B). Conversely, 4R increase would facilitate motor detachment and impair kinesin (Trinczek et al., 1999). This is consistent with the reduction in the anterograde velocities observed in this condition, suggesting a reduced load in the number of active kinesins driving the APP vesicle with no change in runs (Figure 5C). *A priori*, this mechanistic model is consistent with *in vitro* experiments showing that kinesin activity is highly regulated by tau compared with dynein (Vershinin et al., 2007; Dixit et al., 2008; McVicker et al., 2011). Yet, there is an apparent contradiction between our experimental data and previous reports showing that *long* 4R tau is less inhibitory for single kinesin than *short* 3R tau which proposed to be due to an increased static inhibitory state of *short* 3R in artificially stabilized MTs (Dixit et al., 2008; Mcvicker et al., 2014). However, such differential impact on kinesin could be explained by the different number of N-terminal repeats in the tau variants used in those studies (*short* tau= 0N3R, and *long* tau= 2N4R). N-terminal repeats also modulate kinesin velocities; being 0N more inhibitory than 2N, and 3R less inhibitory than 4R (Tarhan et al., 2013). In our system, 3R and 4R tau are not expected to differ in the N-terminal repeats given that the *trans*-splicing reaction occurs at intron 9, spatiotemporally downstream of exons 2 and 3 splicing.

Although we propose a simplified model of tau isoforms affecting motors through their differential binding to MTs (Figure 5), it is noteworthy that such regulation of transport could also arise indirectly, upon changes in other tau isoform-dependent functions, such as the regulation of MT dynamics (Mandelkow et al., 2003), motor stability (Tarhan et al., 2013), the interaction with the dynactin complex (Magnani et al., 2007) and/or the control of kinases involved in the phosphorylation of motors (Kanaan et al., 2012).

Finally, these findings also highlight the relevant physiological role of tau alternative splicing in the human brain. During early development, all mammals express high levels of 3R tau in the nervous system; however, while 4R tau is predominant in the adult brain of most species, the (normal) adult human brain contains equal levels of 3R and 4R tau (Goedert et al., 1989; Andreadis, 2005). A differential anterograde to retrograde bias for 3R and 4R tau in axonal transport is consistent with the predominance of 3R tau during neuronal development that should favor the distal delivery of cargos in projections that need to grow and extend, while the 3R:4R balance reached in mature human neurons would be functional to maintain synapse delivery but also retrieval of survival factors to the soma. The human neurons derived from hESC used in this study displayed an endogenous 4R/3R ratio of 0.6 after 19 days in culture, showing that 3R isoform still predominates over 4R, probably due to the embryonic origin of the neurons and the short time in culture. The *trans*-splicing induced by LV-PTM3R or LV-PTM4R creates an imbalance of tau isoforms leading to significant shifts in the almost equivalent ratio of human derived neurons. Changes in the relative content of 3R and 4R tau have been shown to affect MT assembly and might impair proper

neuronal polarity development (Panda et al., 2003). However, we did not observe significant changes in neuronal morphology or polarization after *trans*-splicing transduction, maybe because the neurons were already highly polarized when tau isoforms shift was induced (DIV 11).

In summary, we provide novel mechanistic data about tau modulation of axonal transport in a relevant human neuronal setting that contribute to understand the highly regulated interplay of molecular motors in microtubule-dependent dynamics. We showed that perturbations in the endogenous 3R:4R tau ratio is sufficient to impair the transport of the Alzheimer's associated molecule APP, suggesting a direct relationship between tau isoforms imbalance and APP *mis*-localization, that might underlie its pathological processing leading to neuronal dysfunction. These data raise new perspectives about the modulation of abnormal tau metabolism as potential therapeutical intervention for human tauopathies, including Alzheimer's disease.

References

Andreadis A (2005) Tau gene alternative splicing: expression patterns, regulation and modulation of function in normal brain and neurodegenerative diseases. Biochim Biophys Acta 1739:91–103.

Avale ME, Rodríguez-Martín T, Gallo JM (2013) Trans-splicing correction of tau isoform imbalance in a mouse model of tau mis-splicing. Hum Mol Genet 22:2603–2611.

Bodea L-G, Eckert A, Ittner LM, Piguet O, Götz J (2016) Tau physiology and pathomechanisms in frontotemporal lobar degeneration. J Neurochem.

601 Bull ND, Guidi A, Goedert M, Martin KR, Spillantini MG (2012) Reduced axonal
602 transport and increased excitotoxic retinal ganglion cell degeneration in mice
603 transgenic for human mutant p301s tau. PLoS One 7:2–9.

604 Dawson HN, Cantillana V, Chen L, Vitek MP (2007) The tau N279K exon 10 splicing
605 mutation recapitulates frontotemporal dementia and parkinsonism linked to
606 chromosome 17 tauopathy in a mouse model. J Neurosci 27:9155–9168.

607 De Vos KJ, Grierson AJ, Ackerley S, Miller CCJ (2008) Role of axonal transport in
608 neurodegenerative diseases. Annu Rev Neurosci 31:151–173.

609 Dixit R, Ross JL, Goldman YE, Holzbaur ELF (2008) Differential regulation of dynein
610 and kinesin motor proteins by tau. Science 319:1086–1089.

611 Ebneth A, Godemann R, Stamer K, Illenberger S, Trinczek B, Mandelkow E (1998)
612 Overexpression of tau protein inhibits kinesin-dependent trafficking of vesicles,
613 mitochondria, and endoplasmic reticulum: implications for Alzheimer's disease. J
614 Cell Biol 143:777–794.

615 Encalada SE, Goldstein LSB (2014) Biophysical challenges to axonal transport: motor-
616 cargo deficiencies and neurodegeneration. Annu Rev Biophys 43:141–169.

617 Falzone TL, Stokin GB (2012) Imaging amyloid precursor protein in vivo: an axonal
618 transport assay. Methods Mol Biol 846:295–303.

619 Falzone TL, Stokin GB, Lillo C, Rodrigues EM, Westerman EL, Williams DS, Goldstein
620 LSB (2009) Axonal stress kinase activation and tau misbehavior induced by
621 kinesin-1 transport defects. J Neurosci 29:5758–5767.

622 Fu M, Holzbaur ELF (2013) JIP1 regulates the directionality of APP axonal transport by
623 coordinating kinesin and dynein motors. J Cell Biol 202:495–508.

624 Ghetti B, Oblak AL, Boeve BF, Johnson K a., Dickerson BC, Goedert M (2015) Invited
625 review: Frontotemporal dementia caused by microtubule-associated protein tau
626 gene (MAPT) mutations: a chameleon for neuropathology and neuroimaging.
627 Neuropathol Appl Neurobiol 41:24–46.

628 Goedert M, Spillantini MG, Jakes R, Rutherford D, Crowther RA (1989) Multiple
629 isoforms of human microtubule-associated protein tau: sequences and localization
630 in neurofibrillary tangles of Alzheimer's disease. Neuron 3:519–526.

631 Goldsbury C, Thies E, Konzack S, Mandelkow E-M (2007) Quantification of amyloid
632 precursor protein and tau for the study of axonal traffic pathways. J Neurosci
633 27:3357–3363.

634 Goldstein LSB (2012) Axonal transport and neurodegenerative disease: can we see the
635 elephant? Prog Neurobiol 99:186–190.

636 Goode BL, Chau M, Denis PE, Feinstein SC (2000) Structural and functional differences
637 between 3-repeat and 4-repeat tau isoforms. Implications for normal tau function
638 and the onset of neurodegenetative disease. J Biol Chem 275:38182–38189.

639 Götz J, Ittner LM, Kins S (2006) Do axonal defects in tau and amyloid precursor protein
640 transgenic animals model axonopathy in Alzheimer's disease? J Neurochem
641 98:993–1006.

642 Hendricks AG, Holzbaur ELF, Goldman YE (2012) Force measurements on cargoes in

643 living cells reveal collective dynamics of microtubule motors. Proc Natl Acad Sci U
644 S A 109:18447–18452.

645 Hutton M et al. (1998) Association of missense and 5'-splice-site mutations in tau with
646 the inherited dementia FTDP-17. Nature 393:702–705.

647 Iovino M, Agathou S, González-Rueda A, Del Castillo Velasco-Herrera M, Borroni B,
648 Alberici A, Lynch T, O'Dowd S, Geti I, Gaffney D, Vallier L, Paulsen O, Káradóttir
649 RT, Spillantini MG (2015) Early maturation and distinct tau pathology in induced
650 pluripotent stem cell-derived neurons from patients with MAPT mutations. Brain
651 138:3345–3359.

652 Iovino M, Pfisterer U, Holton JL, Lashley T, Swingler RJ, Calo L, Treacy R, Revesz T,
653 Parmar M, Goedert M, Muqit MMK, Spillantini MG (2014) The novel MAPT
654 mutation K298E: Mechanisms of mutant tau toxicity, brain pathology and tau
655 expression in induced fibroblast-derived neurons. Acta Neuropathol 127:283–295.

656 Ittner LM, Fath T, Ke YD, Bi M, van Eersel J, Li KM, Gunning P, Götz J (2008)
657 Parkinsonism and impaired axonal transport in a mouse model of frontotemporal
658 dementia. Proc Natl Acad Sci U S A 105:15997–16002.

659 Kanaan NM, Morfini G, Pigino G, LaPointe NE, Andreadis A, Song Y, Leitman E, Binder
660 LI, Brady ST (2012) Phosphorylation in the amino terminus of tau prevents
661 inhibition of anterograde axonal transport. Neurobiol Aging 33:826

662 Ke YD, Suchowerska AK, Van Der Hoven J, De Silva DM, Wu CW, Van Eersel J, Ittner
663 A, Ittner LM (2012) Lessons from Tau-deficient mice. Int J Alzheimers Dis 2012.

664 Koo EH, Sisodia SS, Archer DR, Martin LJ, Weidemann A, Beyreuther K, Fischer P,
665 Masters CL, Price DL (1990) Precursor of amyloid protein in Alzheimer disease
666 undergoes fast anterograde axonal transport. Proc Natl Acad Sci U S A 87:1561–
667 1565.
668 Leidel C, Longoria RA, Gutierrez FM, Shubeita GT (2012) Measuring molecular motor
669 forces in vivo: implications for tug-of-war models of bidirectional transport. Biophys
670 J 103:492–500.
671 Ma Q-L, Zuo X, Yang F, Ubeda OJ, Gant DJ, Alaverdyan M, Kiosea NC, Nazari S, Chen
672 PP, Nothias F, Chan P, Teng E, Frautschy S a, Cole GM (2014) Loss of MAP
673 function leads to hippocampal synapse loss and deficits in the Morris Water Maze
674 with aging. J Neurosci 34:7124–7136.
675 Magnani E, Fan J, Gasparini L, Golding M, Williams M, Schiavo G, Goedert M, Amos
676 LA, Spillantini MG (2007) Interaction of tau protein with the dynactin complex.
677 EMBO J 26:4546–4554.
678 McVicker DP, Chrin LR, Berger CL (2011) The nucleotide-binding state of microtubules
679 modulates kinesin processivity and the ability of Tau to inhibit kinesin-mediated
680 transport. J Biol Chem 286:42873–42880.
681 Mcvicker DP, Hoeprich GJ, Thompson AR, Berger CL (2014) Tau interconverts
682 between diffusive and stable populations on the microtubule surface in an isoform
683 and lattice specific manner. Cytoskeleton 71:184–194.
684 Mellone M, Kestoras D, Andrews MR, Dassie E, Crowther RA, Stokin GB, Tinsley J,
685 Horne G, Goedert M, Tolkovsky AM, Spillantini MG (2013) Tau pathology is present

in vivo and develops in vitro in sensory neurons from human P301S tau transgenic mice: a system for screening drugs against tauopathies. J Neurosci 33:18175–18189.

Mertens J, Stüber K, Poppe D, Doerr J, Ladewig J, Brüstle O, Koch P (2013) Embryonic stem cell-based modeling of tau pathology in human neurons. Am J Pathol 182:1769–1779.

Morris M, Maeda S, Vossel K, Mucke L (2011) The many faces of tau. Neuron 70:410–426.

Müller MJI, Klumpp S, Lipowsky R (2008) Tug-of-war as a cooperative mechanism for bidirectional cargo transport by molecular motors. Proc Natl Acad Sci U S A 105:4609–4614.

Otero MG, Alloatti M, Cromberg LE, Almenar-Queralt A, Encalada SE, Pozo Devoto VM, Bruno L, Goldstein LSB, Falzone TL (2014) Fast axonal transport of the proteasome complex depends on membrane interaction and molecular motor function. J Cell Sci 127:1537–1549.

Panda D, Samuel JC, Massie M, Feinstein SC, Wilson L (2003) Differential regulation of microtubule dynamics by three- and four-repeat tau: implications for the onset of neurodegenerative disease. Proc Natl Acad Sci U S A 100:9548–9553.

Reis GF, Yang G, Szpankowski L, Weaver C, Shah SB, Robinson JT, Hays TS, Danuser G, Goldstein LSB (2012) Molecular motor function in axonal transport in vivo probed by genetic and computational analysis in Drosophila. Mol Biol Cell

23:1700–1714.

Rodriguez-Martin T, Garcia-Blanco MA, Mansfield SG, Grover AC, Hutton M, Yu Q, Zhou J, Anderton BH, Gallo JM (2005) Reprogramming of tau alternative splicing by spliceosome-mediated RNA trans-splicing: implications for tauopathies. Proc Natl Acad Sci U S A 102:15659–15664.

Rodríguez-Martín T, Pooler AM, Lau DHW, Mórotz GM, De Vos KJ, Gilley J, Coleman MP, Hanger DP (2016) Reduced number of axonal mitochondria and tau hypophosphorylation in mouse P301L tau knockin neurons. Neurobiol Dis 85:1–10.

Spillantini MG, Goedert M (2013) Tau pathology and neurodegeneration. Lancet Neurol 12:609–622.

Spillantini MG, Murrell JR, Goedert M, Farlow MR, Klug A, Ghetti B (1998) Mutation in the tau gene in familial multiple system tauopathy with presenile dementia. Proc Natl Acad Sci U S A 95:7737–7741.

Stamer K, Vogel R, Thies E, Mandelkow E, Mandelkow EM (2002) Tau blocks traffic of organelles, neurofilaments, and APP vesicles in neurons and enhances oxidative stress. J Cell Biol 156:1051–1063.

Stokin GB, Lillo C, Falzone TL, Brusch RG, Rockenstein E, Mount SL, Raman R, Davies P, Masliah E, Williams DS, Goldstein LSB (2005) Axonopathy and transport deficits early in the pathogenesis of Alzheimer's disease. Science 307:1282–1288.

Tarhan MC, Orazov Y, Yokokawa R, Karsten SL, Fujita H (2013) Biosensing MAPs as "roadblocks": kinesin-based functional analysis of tau protein isoforms

728 and mutants using suspended microtubules (sMTs). Lab Chip 13:3217–3224.

729 Terada S, Kinjo M, Aihara M, Takei Y, Hirokawa N (2010) Kinesin-1/Hsc70-dependent
730 mechanism of slow axonal transport and its relation to fast axonal transport. EMBO
731 J 29:843–854.

732 Trinczek B, Ebneth a, Mandelkow EM, Mandelkow E (1999) Tau regulates the
733 attachment/detachment but not the speed of motors in microtubule-dependent
734 transport of single vesicles and organelles. J Cell Sci 112 (Pt 1:2355–2367.

735 Vershinin M, Carter BC, Razafsky DS, King SJ, Gross SP (2007) Multiple-motor based
736 transport and its regulation by Tau. Proc Natl Acad Sci U S A 104:87–92.

737 Yuan A, Kumar A, Duff K, Nixon R a. (2013) Global axonal transport rates are unaltered
738 in htau mice in vivo. J Alzheimer's Dis 37:579–586.

739 Yuan A, Kumar A, Peterhoff C, Duff K, Nixon RA (2008) Axonal transport rates in vivo
740 are unaffected by tau deletion or overexpression in mice. J Neurosci 28:1682–
741 1687.

742 Zhang XQ, Zhang SC (2010) Differentiation of neural precursors and dopaminergic
743 neurons from human embryonic stem cells. Methods Mol Biol. 584:355-66.

744

745 **Figure Legends**

746 **Figure 1: 3R or 4R tau modulation by *trans*-splicing in highly polarized human**
747 **neurons. A-B)** Human neuronal cultures at five days after plating (DIV 5) showing
748 projections and proper polarization in brigthfield (A) and after immunostaining with
749 axonal and dendritic markers (Tau and MAP2) (B). White arrow indicates the axon
750 without MAP2 staining and yellow arrows show dendrites. **C)** Enriched human neuronal
751 cultures at DIV 18, showing highly polarized projections and dense connectivity. **D)**
752 Neuron at DIV 19 showing co-localization of APP-YFP (green) with LV-dsRED
753 transduction (red). **E)** Map of lentiviral vectors (LV) used for neuronal transduction at
754 DIV 11. LV-dsRED: control vector carrying the reporter cassette; LV-PTM3R: LV
755 carrying a pre-*trans*-splicing molecule with exons 11-13; or LV-PTM4R: with exons 10-
756 13. TSD: *trans*-splicing domain consisting of a binding domain complementary to the 3'
757 end of intron 9, a branch point and a 3' splice acceptor site. **F)** Representative gel of
758 RT-PCR products obtained with primers spanning tau exons 9-13, simultaneously
759 amplifying 3R and 4R isoforms. RT-PCR was performed with mRNA extracted from
760 neurons transduced with each LV. **G)** Relative content of 3R and 4R tau isoforms,
761 determined by real time RT-PCR with specific primers for 3R (E10-) and 4R (E10+) tau
762 mRNA. Delta Ct was calculated relative to human ApoB gene expression (mean
763 ±S.E.M; n=3), in three independent experiments. One-way ANOVA followed by
764 Dunnet's comparison *versus* control neurons, performed separately for each isoform;
765 *p<0.05 and **p<0.001 *versus* 3R CTRL; $^{\#}p$<0.001 *vs* 4R CTRL. **H-I)** Western blot
766 analyses of human neurons homogenates. Detection of 3R (H) and 4R (I) tau protein
767 with isoform-specific antibodies normalized to actin, quantified by optical density;

768 **p<0.001 (n=3); One-way ANOVA followed by Dunnett's comparison to control (CTRL)
769 neurons (transduced with LV-dsRED).

770

771 **Figure 2: Normal neuronal polarization after 3R:4R tau isoform modulation. A)**
772 Confocal images of enriched neuronal cultures at DIV 19 without transduction, or
773 transduced with LV-PTM3R or LV-PTM4R (from top to bottom). Immunofluorescence
774 staining showing APP, tau and Hoechst number for nuclei. **B)** Confocal high
775 magnification images from control and transduced neurons stained for APP and tau
776 showing polarization and extension integrity. **C-D)** Sum of neuronal projection extension
777 expressed in µm (H), and number of primary projection extensions from cell bodies (I) in
778 neurons at DIV 19 that were transduced at DIV 11 with LV control, LV-PTM3R and LV-
779 PTM4R. **E)** Sholl analysis performed at DIV 19 in transduced neurons showing the
780 number of projection intersections *versus* distance from cell bodies (µm) (Data
781 represent mean ± S.E.M; n=10). **F-G)** Western blot of neuronal homogenates showing
782 total tau and APP protein levels after each LV transduction conditions compared to non-
783 transduced control (NTC) neurons. Tubulin (tub) was used as loading control. (Data in
784 G is expressed as percentage of NTC; mean ±S.E.M; n=3). **H)** Western blot using
785 antibodies specific to tau phosphorylated at Ser 202 (CP13) or Ser 396/404 (PHF-1).
786 Quantitative analyses are related to beta-actin signal as loading control (mean ±S.E.M;
787 n=3).

788

789 **Figure 3: Impairment of axonal transport of APP vesicles in neurons after under**
790 **tau 3R:4R imbalance. A)** Representative images from movies used to analyze the

axonal transport of APP vesicles in neurons transduced with LV-control (dsRED), LV-PTM3R and LV-PTM4R. Scale bar: 10 µm. See movies 1-3 **B)** Kymographs of time versus distance from a 30s movie generated at 8 frames/s in axons from neurons transfected with APP-YFP Scale bar: 10 µm. **C)** Average proportion per kymographs of anterograde, stationary and retrograde APP-YFP vesicles from non-transduced control (NTC), or transduced with LV carrying dsRED, PTM3R or PTM4R. **D)** Average velocity of anterograde and retrograde moving vesicles per kymographs. kymographs analyzed *n*= 59 (NTC); 78 (dsRED); 57 (PTM3R); 58 (PTM4R). One-way ANOVA followed by Dunnett's comparison *versus* NTC *<0.05, **<0.02, ***<0.01. **E)** Average number of APP-YFP vesicles per µm of axonal length in NTC, dsRED, PTM3R and PTM4R. *n*= 25 for each. One-way ANOVA.

Figure 4: Kinesin and dynein transport properties are differentially impaired by tau isoform ratio modulation in human neurons. A) Representative kymographs of time versus distance showing moving and stationary APP vesicles and their trajectories using MATLAB (dotted lines). **B)** Representative recovered trajectory plotted as a function of distance *vs* time showing the properties extracted using custom made MATLAB scripts. **C-E**) Run lengths, segmental velocities, pauses and reversions were determined from a total of 1283 trajectories (see methods for details). **C)** Anterograde and retrograde average run lengths of vesicles moving in a net direction, obtained from APP-YFP trajectories in neurons transduced with LV-dsRED (control), PTM3R or PTM4R. *n*= ctrl: antero 1551, retro 1548; PTM3R: antero 572, retro 555; PTM4R: antero 465, retro 503. One-way ANOVA followed by Dunnet's comparison *versus* Ctrl *<0.05,

***<0.01. **D)** Average number of pauses and reversions per trajectory. Pauses *n*= ctrl: 2752; PTM3R: 981; PTM4R: 913. Reversion: *n*= ctrl: 895; PTM3R: 307; PTM4R: 262. **E-H)** Distribution of segmental velocities of moving APP-YFP vesicles. A Gaussian mixture model with 3 modes (A, B and C) was used to represent the segmental velocities distributions for anterograde (E) and retrograde (G) APP vesicle transport in control (full line), or transduced with PTM3R (light grey) or PTM4R (dark grey) LVs (dotted lines). The center and fraction of the different modes are displayed in Table I. Relative frequencies of anterograde (F) and retrograde (H) segmental velocities used for model construction. Segmental velocities *n*= ctrl: antero 1671, retro 1344; PTM3R: antero 795, retro 549; PTM4R: antero 916, retro 752. Significant differences (**) obtained from comparison of non-overlapping confidence intervals to control group (LV-dsRED transduced neurons).

Figure 5: Hybrid competition-regulation model of tau isoform-dependent APP axonal transport. We propose a model where the APP vesicle is driven by two groups of motors –i.e. kinesin and dynein- along tau-decorated MTs. Motors behave in a tug-of-war/coordination scenario; displaying a differential tau isoform-dependent interaction with MTs. **A)** In control condition the two groups of motors are balanced to result in higher anterograde runs (dark arrows) and segmental velocities (light arrows) compared to the retrograde ones giving an anterograde bias (red triangle) for the movement of APP vesicles. **B)** Shifts in the ratio towards 3R would not change the amount of tau bound to MT but reduce its binding strength, facilitating the recruitment of extra active motors. Extra kinesin load leads to an anterograde bias (red triangle) that favors the

distal delivery of APP vesicles. **C)** Increased 4R tau level induces a higher binding strength of tau to MT that facilitate anterograde motor detachment and strongly impair kinesin velocities (light arrows) while no significant changes in retrograde runs or velocities are observed. This results in a retrograde bias (red triangle) that should favor retrieval of APP vesicles to the cell body.

Table I. Segmental velocity data modeled as a combination of normal distributions. The table displays the values of the central position and fraction? of the modes parameters of a Gaussian mixture model with three components (A, B and C) obtained using an Expectation Maximization algorithm. Errors were determined as the standard deviation of n=1000 resampling with replacements bootstrapping procedure. Significant differences (**) obtained from comparison of non overlapping confidence intervals to control group (LV-dsRED transduced neurons).

Movie 1: APP transport in control neuron: Representative movie showing the axonal transport of APP vesicles in real time in a neuron that has been transduced with control lentivirus and transfected with APP-YFP. Movie showing time in seconds (8 frames/s) is oriented so right to left moving vesicles corresponds to anterograde transport, and left to right to retrograde movement. Scale bar: 20 μm.

Movie 2: APP transport in PTM3R transduced neuron: Representative movie showing axonal transport of APP vesicles in real time in a neuron that has been

transduced with PTM3R lentivirus and transfected with APP-YFP. Movie showing time in seconds (8 frames/s) is oriented so right to left moving vesicles corresponds to anterograde axonal transport, and left to right to retrograde movement. Scale bar: 20 µm.

Movie 3: APP transport in PTM4R transduced neuron: Representative movie showing the axonal transport of APP vesicles in real time in a neuron that has been transduced with PTM4R lentivirus and transfected with APP-YFP. Movie showing time in seconds (8 frames/s) is oriented so right to left moving vesicles corresponds to anterograde axonal transport, and left to right to retrograde movement. Scale bar: 20 µm.

Figure 1:

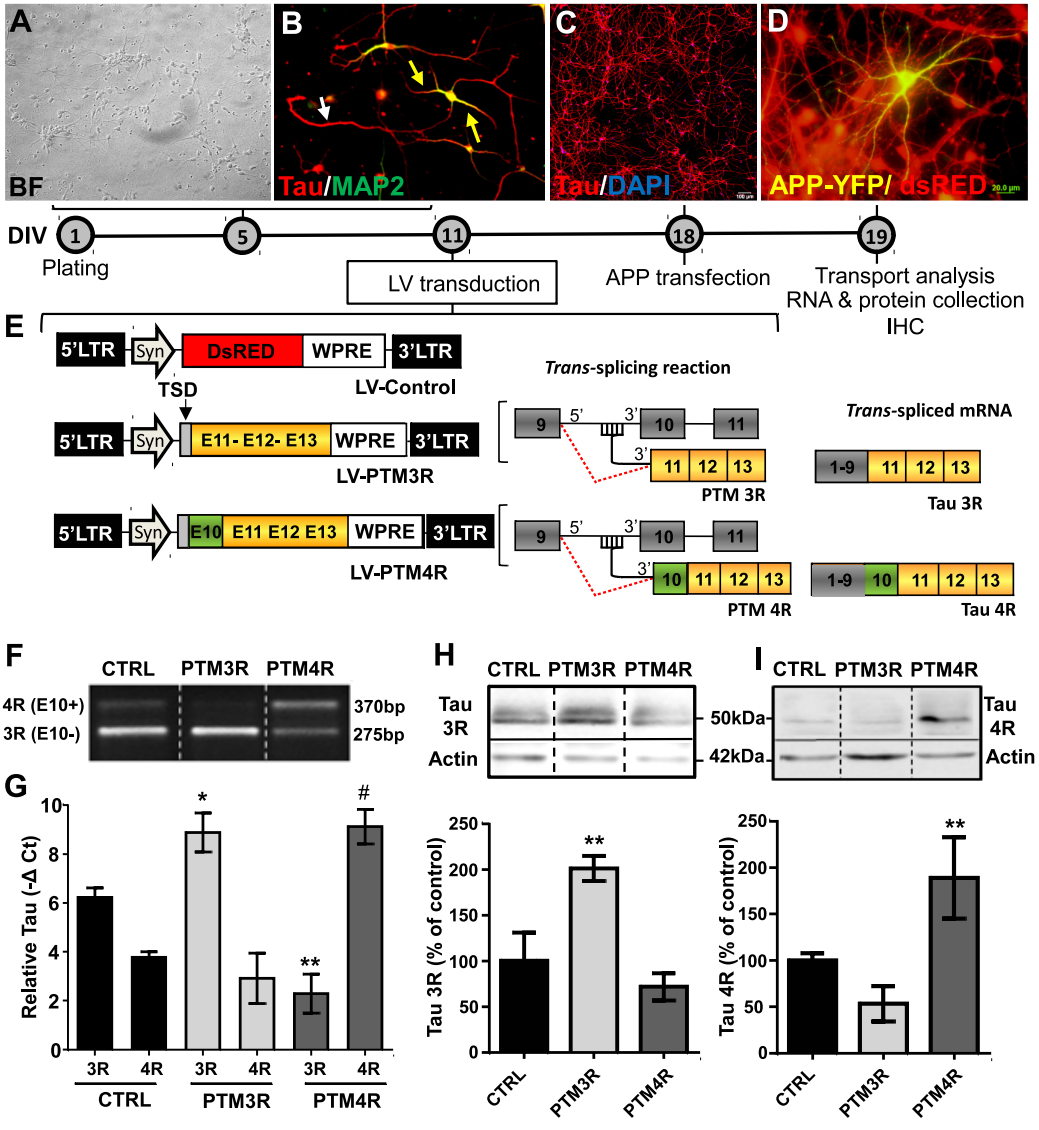

Figure 2:

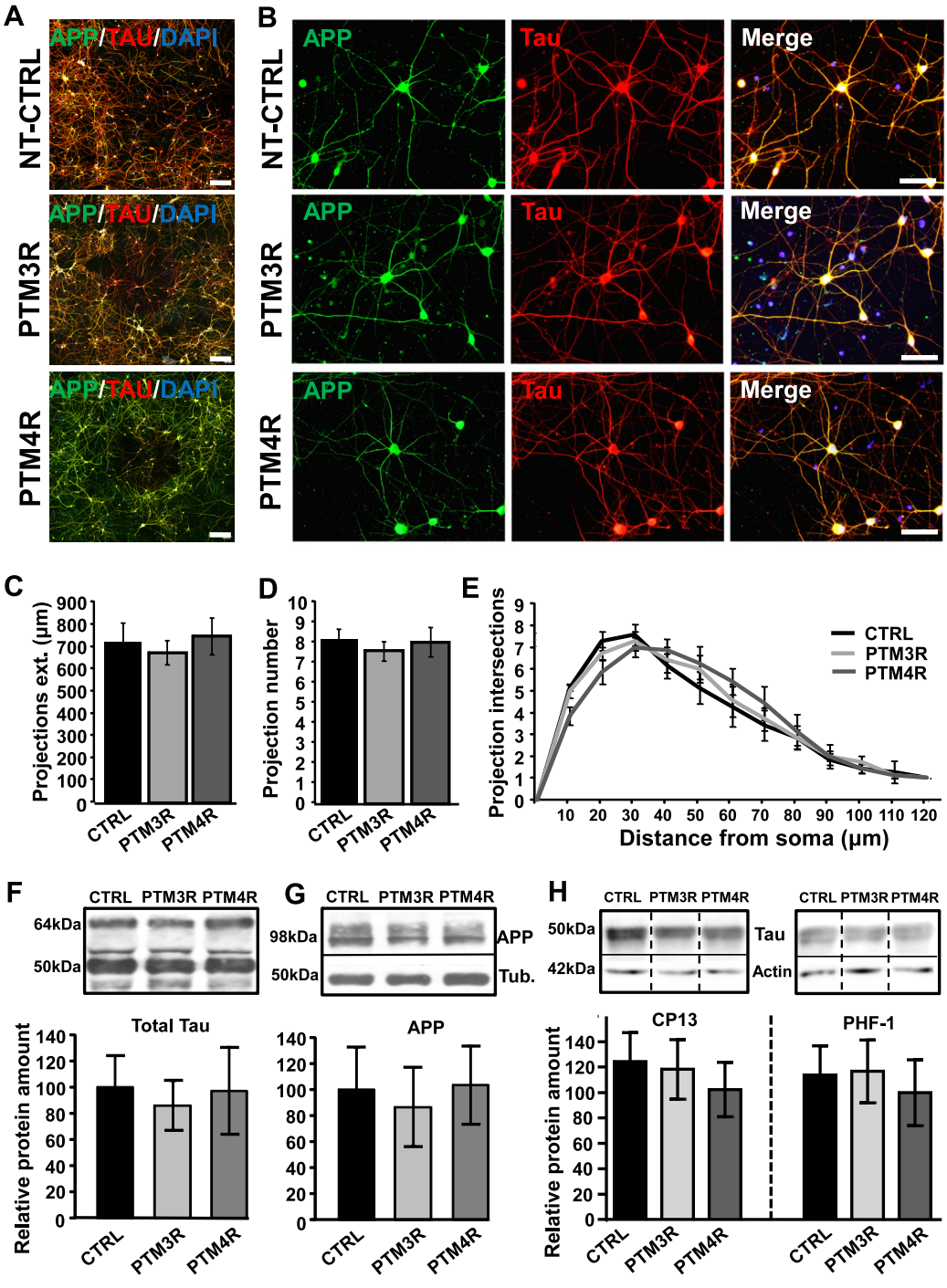

Figure 3:

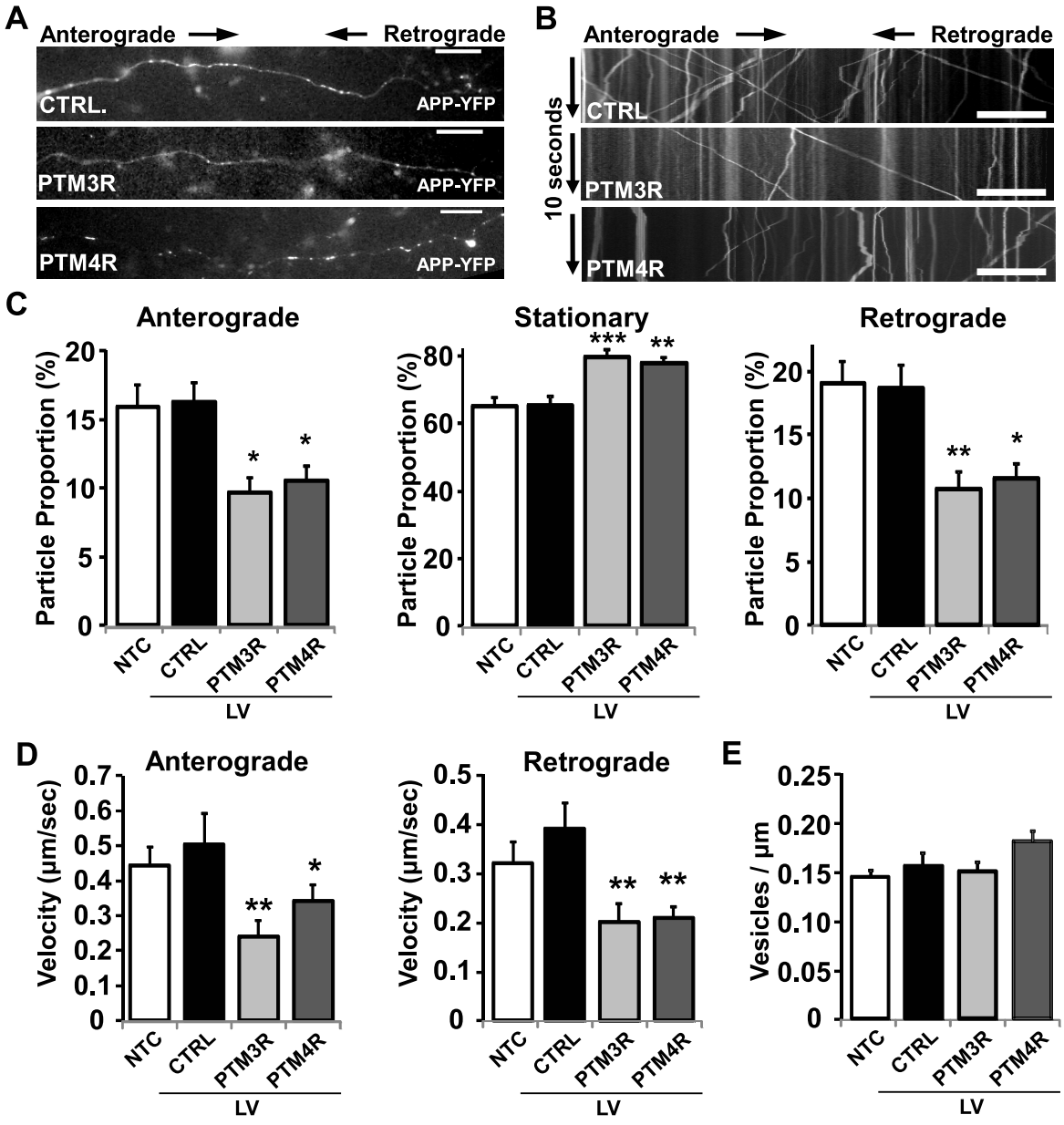

Figure 4:

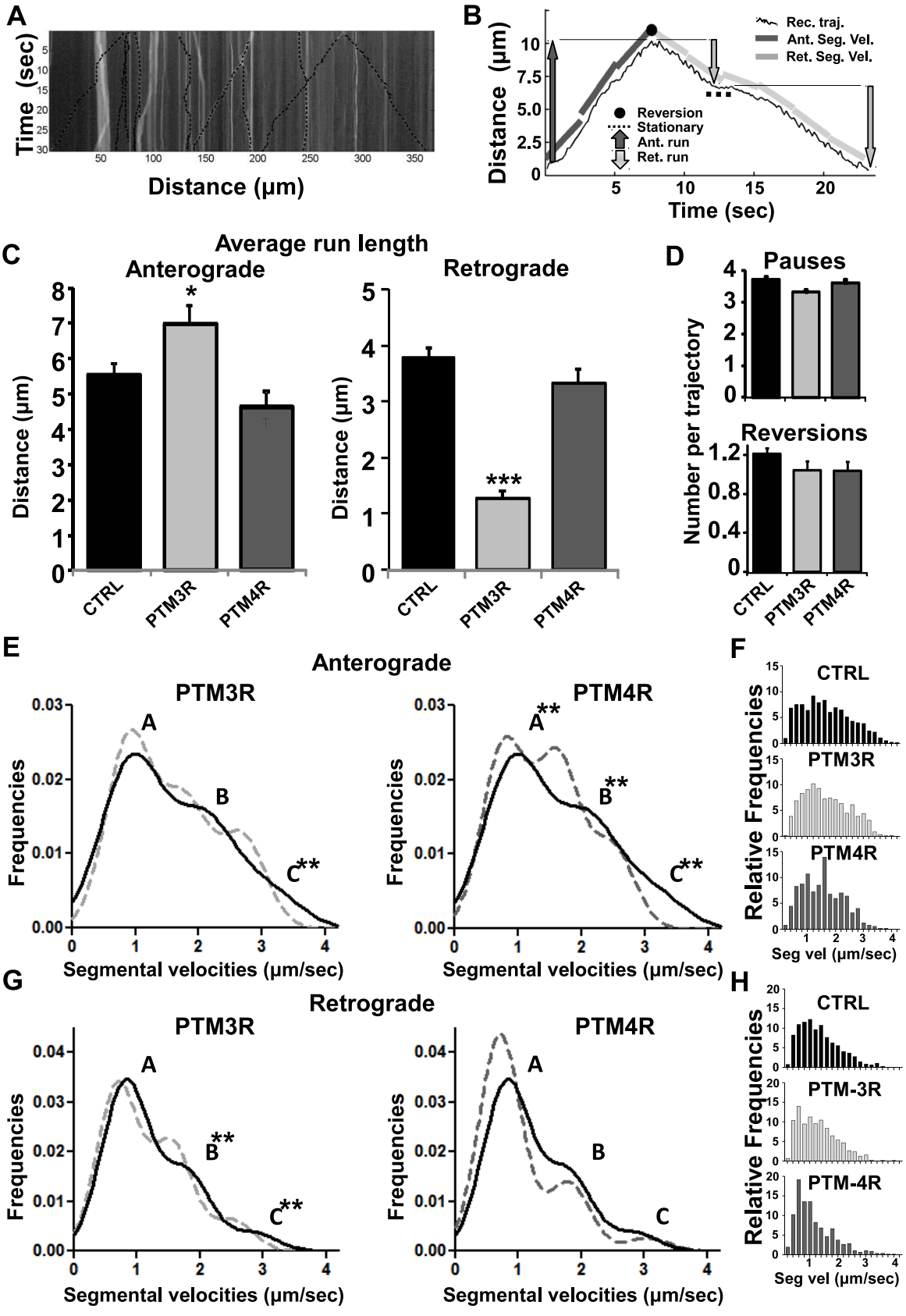

Figure 5:

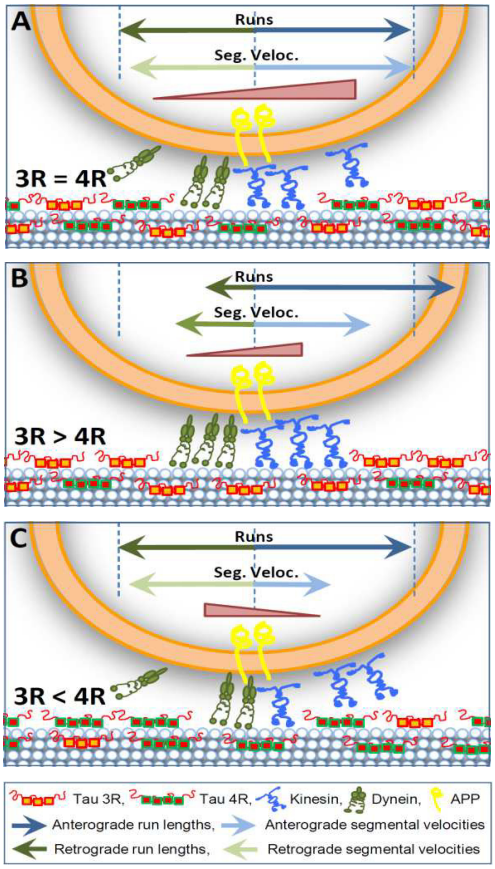

Table 1

ANTEROGRADE

Mode Center

	A Max +/- error	B Max +/- error	C Max +/- error
PTM-dsRED	**0.94** +/- 0.07	**2.09** +/- 0.19	**3.11** +/- 0.38
PTM-3R	**0.90** +/- 0.04	**1.77** +/- 0.09	**2.69** +/- 0.06 **
PTM-4R	**0.78** +/- 0.07 **	**1.62** +/- 0.13 **	**2.49** +/- 0.16 **

Mode Fraction

	A Mode	B Mode	C Mode	error	Sigma +/- error
PTM-dsRED	**0.54**	**0.34**	**0.12**	+/- 0.05	0.24 +/- 0.04
PTM-3R	**0.47**	**0.31**	**0.23**	+/- 0.03	0.13 +/- 0.02
PTM-4R	**0.42**	**0.39**	**0.19**	+/- 0.05	0.12 +/- 0.03

RETROGRADE

Mode Center

	A Max +/- error	B Max +/- error	C Max +/- error
PTM-dsRED	**0.81** +/- 0.03	**1.78** +/- 0.09	**2.88** +/- 0.14
PTM-3R	**0.69** +/- 0.04	**1.55** +/- 0.09 **	**2.52** +/- 0.14 **
PTM-4R	**0.71** +/- 0.02	**1.78** +/- 0.10	**3.04** +/- 0.18

Mode Fraction

	A Mode	B Mode	C Mode	error	Sigma +/- error
PTM-dsRED	**0.64**	**0.29**	**0.07**	+/- 0.03	0.14 +/- 0.01
PTM-3R	**0.55**	**0.35**	**0.10**	+/- 0.04	0.11 +/- 0.02
PTM-4R	**0.72**	**0.23**	**0.05**	+/- 0.02	0.11 +/- 0.01